Обзор ArXiv/astro-ph, 15-21 декабря 2016

От Сильченко О.К.

Astro-ph: 1612.06495

TESTING THE PRESENCE OF MULTIPLE PHOTOMETRIC COMPONENTS IN NEARBY EARLY-TYPE GALAXIES USING SDSS

Semyeong Oh[1,3], Jenny E. Greene[1] and Claire N. Lackner[2]

Draft version December 21, 2016

ABSTRACT

We investigate two-dimensional image decomposition of nearby, morphologically selected early-type galaxies (ETGs). We are motivated by recent observational evidence of significant size growth of quiescent galaxies and theoretical development advocating a two-phase formation scenario for ETGs. We find that a significant fraction of nearby ETGs show changes in isophotal shape that require multi-component models. The characteristic sizes of the inner and outer component are ~ 3 and ~ 15 kpc. The inner component lies on the mass-size relation of ETGs at $z \sim 0.25 - 0.75$, while the outer component tends to be more elliptical and hints at a stochastic buildup process. We find real physical differences between the single- and double-component ETGs, with the double-component galaxies being younger and more metal-rich. The fraction of double component ETGs increases with increasing σ and decreases in denser environments. We hypothesize that double-component systems

Выборка

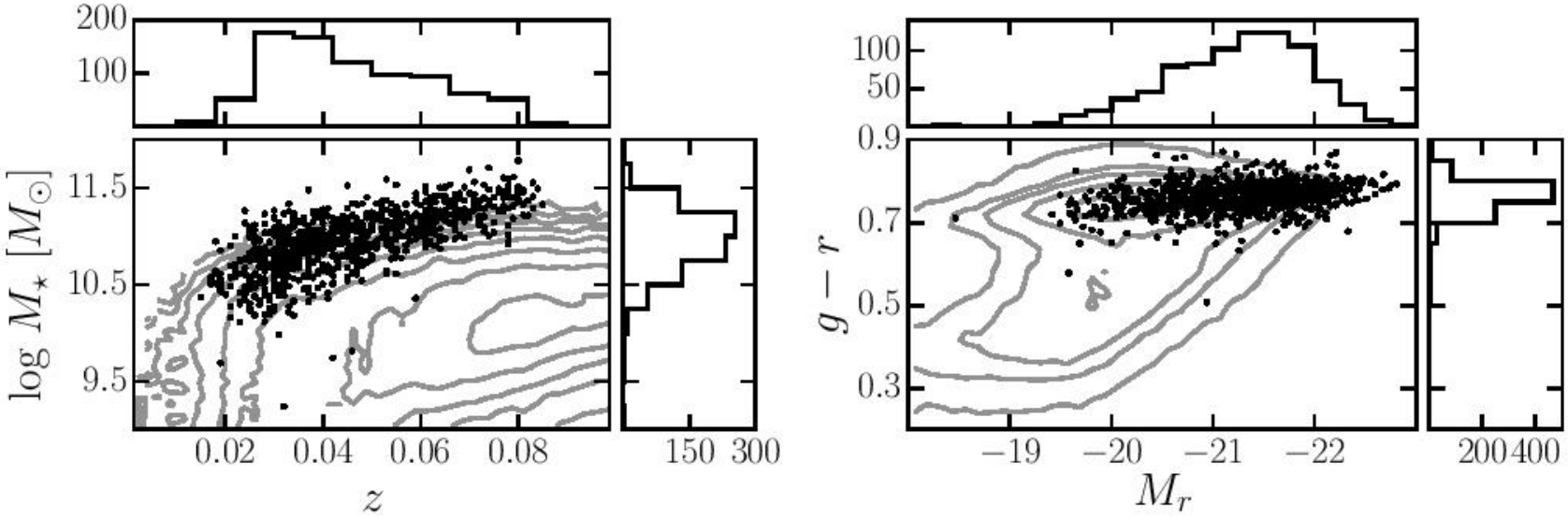

FIG. 1.— Distribution of the sample galaxies (black dots) in the redshift vs. $\log M_\star$ plane (left) and $(g-r)$ vs. M_r color-magnitude diagram (right). In each panel, we show the distribution of SDSS galaxies in the NYU-VAGC (Blanton et al. 2005) at $z < 0.1$ as gray contours with logarithmic spacing. Histograms show the distribution of each parameter for the sample only.

Пример декомпозиции

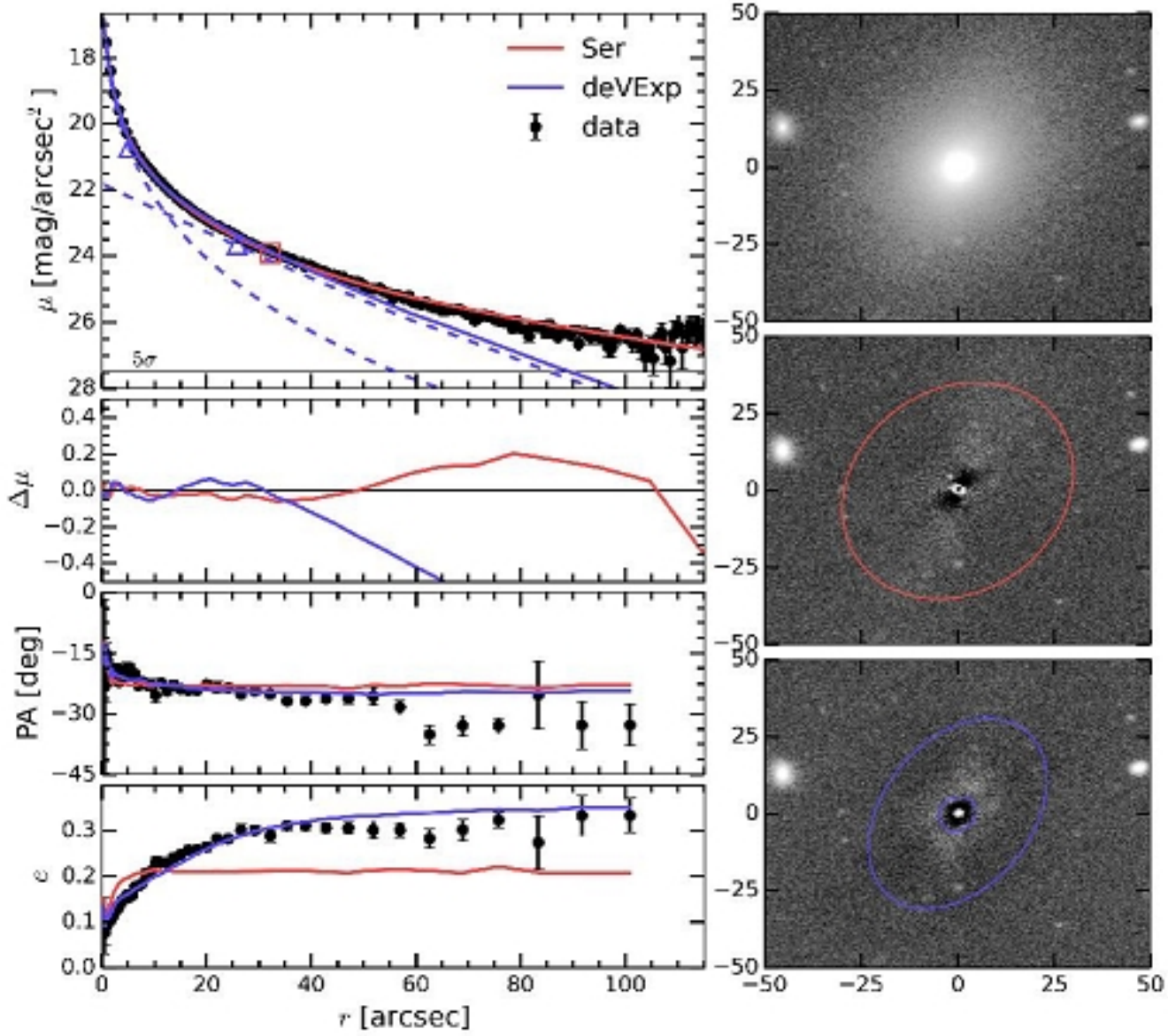

Распределения изофотных параметров

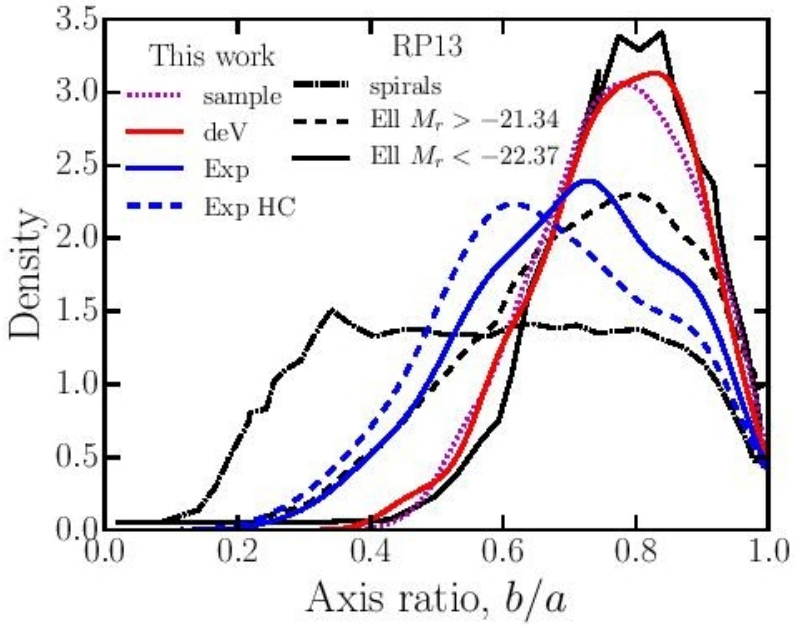

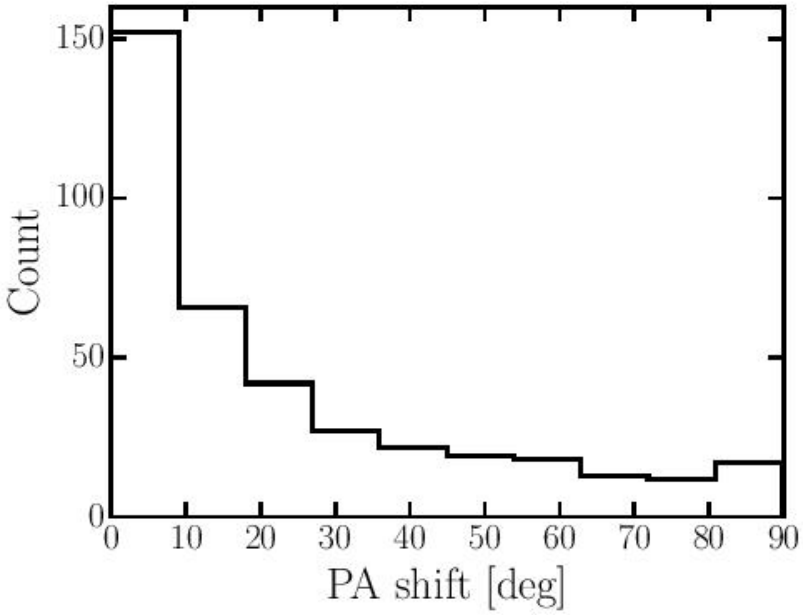

FIG. 11.— Histogram of the PA shift between the deV and Exp component of the deVExp model for double component ETGs.

Результаты

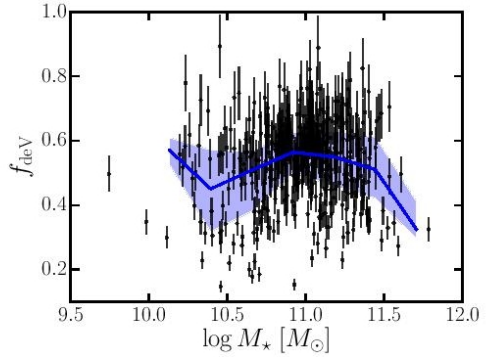

FIG. 12.— Flux fraction of inner deV component as a function of total stellar mass. We show the median and $25-75$ percentiles in equally spaced $\log M_\star$ bins from 10 to 12 with the blue solid line and shaded regions.

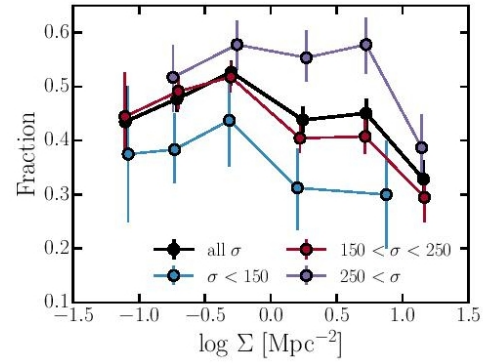

FIG. 15.— Fraction of double component ETGs as a function of projected neighbor density (Baldry et al. 2006). We show the trend in bins of σ. There is a weak trend towards a decreasing double component fraction with increasing galaxy densities.

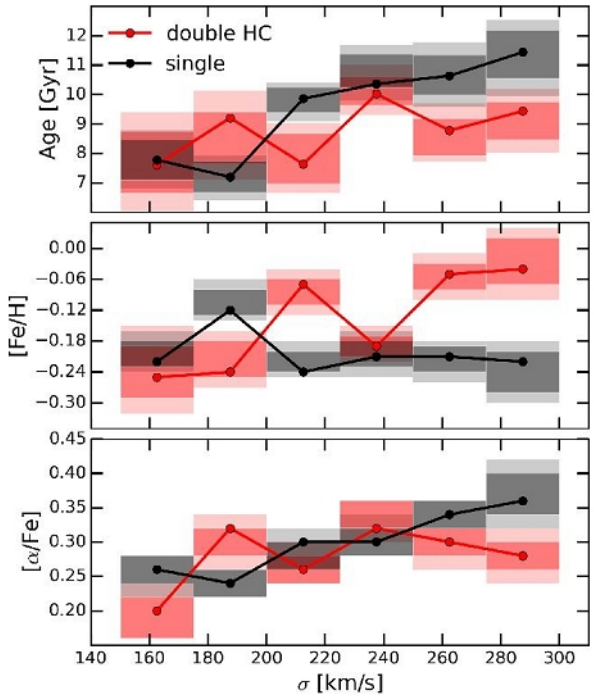

Сценарий: центральный сфероид – к z=0.75

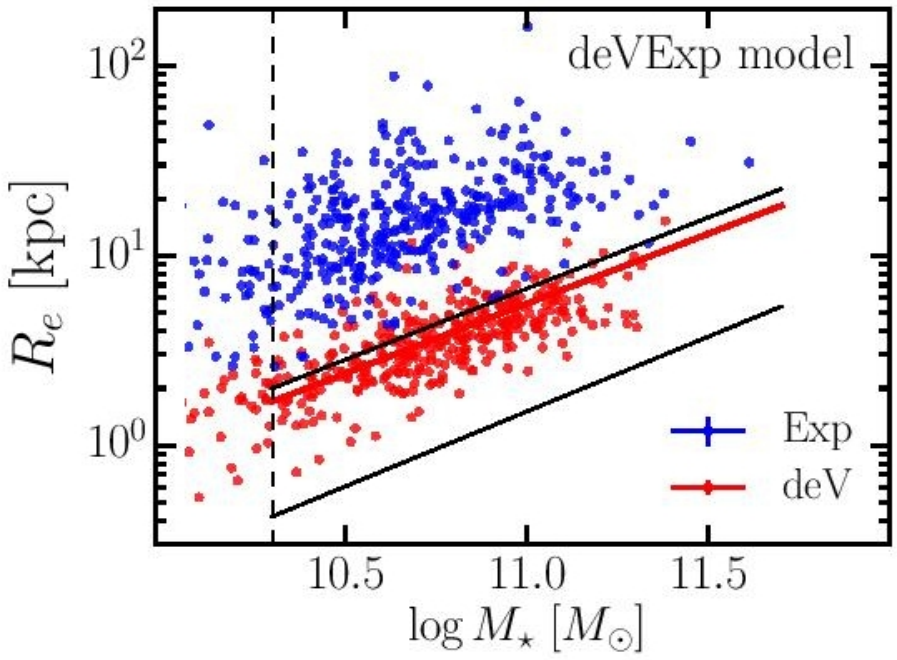

Astro-ph: 1612.05262

THE SIZE EVOLUTION OF STAR-FORMING GALAXIES SINCE $Z \sim 7$ USING ZFOURGE

Rebecca J. Allen[1,3], Glenn G. Kacprzak[1], Karl Glazebrook[1], Ivo Labbé[5], Kim-Vy H. Tran[2], Lee R. Spitler[3,4], Michael Cowley[3,4], Themiya Nanayakkara[1], Casey Papovich[2], Ryan Quadri[2], Caroline M. S. Straatman[6], Vithal Tilvi[2], Pieter van Dokkum[7]

Draft version December 19, 2016

ABSTRACT

For the first time, we present the size evolution of a mass-complete ($\log(M_*/\mathrm{M}_\odot)$>10) sample of star-forming galaxies over redshifts $z = 1 - 7$, selected from the FourStar Galaxy Evolution Survey (ZFOURGE). Observed H-band sizes are measured from the Cosmic Assembly Near-Infrared Deep Extragalactic Legacy Survey (CANDELS) Hubble Space Telescope (*HST*)/F160W imaging. Distributions of individual galaxy masses and sizes illustrate that a clear mass−size relation exists up to $z \sim 7$. At $z \sim 7$, we find that the average galaxy size from the mass−size relation is more compact at a fixed mass of $\log(M_*/\mathrm{M}_\odot) = 10.1$, with $r_{1/2,maj} = 1.02 \pm 0.29$ kpc, than at lower redshifts. This is consistent with our results from stacking the same CANDELS *HST*/F160W imaging, when we correct for galaxy position angle alignment. We find that the size evolution of star-forming galaxies is well fit by a power law of the form $r_e = 7.07(1+z)^{-0.89}$ kpc, which is consistent with previous works for

Эволюция размеров

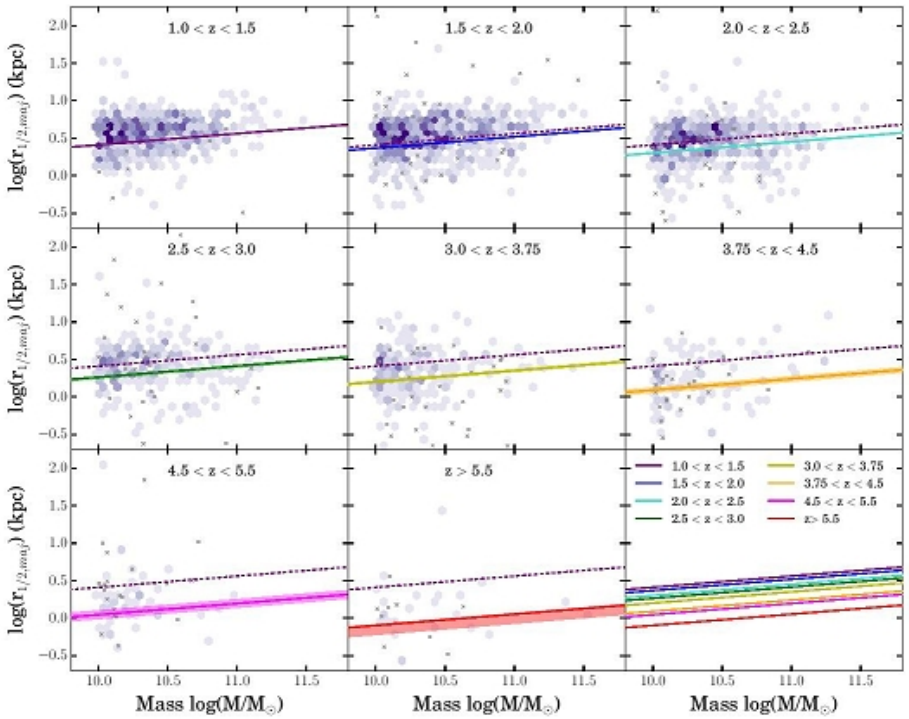

Figure 1. Galaxy stellar mass–size distributions for star-forming galaxies for redshifts $1<z<7.2$. In each panel, galaxies with reliable fits from GALFIT are shown as purple points, while galaxies with poor fits are shown as grey crosses, which are not included in the fits. We fit each distribution following $r\ (m_*)/kpc = r_0 \cdot m_*^{0.15}$, which is shown as a contour including the 1σ errors. The best-fit for $r_{1/2,maj}$ decreases with redshift, which we demonstrate by including the lowest redshift fit in panels with $z>1.5$ as a dashed purple line. In the last panel, we include the fitted mass–size relation from all redshifts using the same colored lines, showing the redshift evolution of galaxy sizes.

Table 1
Best-fit values for A, mass-normalised average sizes, and average sizes from image stacks.

	Fit*			Stack$^{**}_{Corr.}$		
Redshift	r_0	$r_{1/2,maj}$ (kpc)	N_{fit}	$r_{1/2,maj}$ (kpc)	Corr. %	N_{stack}
$1.0<z<1.5$	0.52	3.28 ± 0.07	542	3.43 ± 0.10	21	563
$1.5<z<2.0$	0.47	2.96 ± 0.07	645	3.23 ± 0.12	22	708
$2.0<z<2.5$	0.41	2.55 ± 0.07	508	2.78 ± 0.06	21	584
$2.5<z<3.0$	0.37	2.34 ± 0.13	254	2.56 ± 0.23	18	327
$3.0<z<3.75$	0.31	2.02 ± 0.10	201	1.88 ± 0.10	22	289
$3.75<z<4.5$	0.20	1.57 ± 0.14	89	1.66 ± 0.10	22	146
$4.5<z<5.5$	0.15	1.42 ± 0.18	53	1.20 ± 0.07	22	89
$5.5<z<7.2$	0.01	1.02 ± 0.29	27	0.93 ± 0.09	17	41

Сложенные изображения

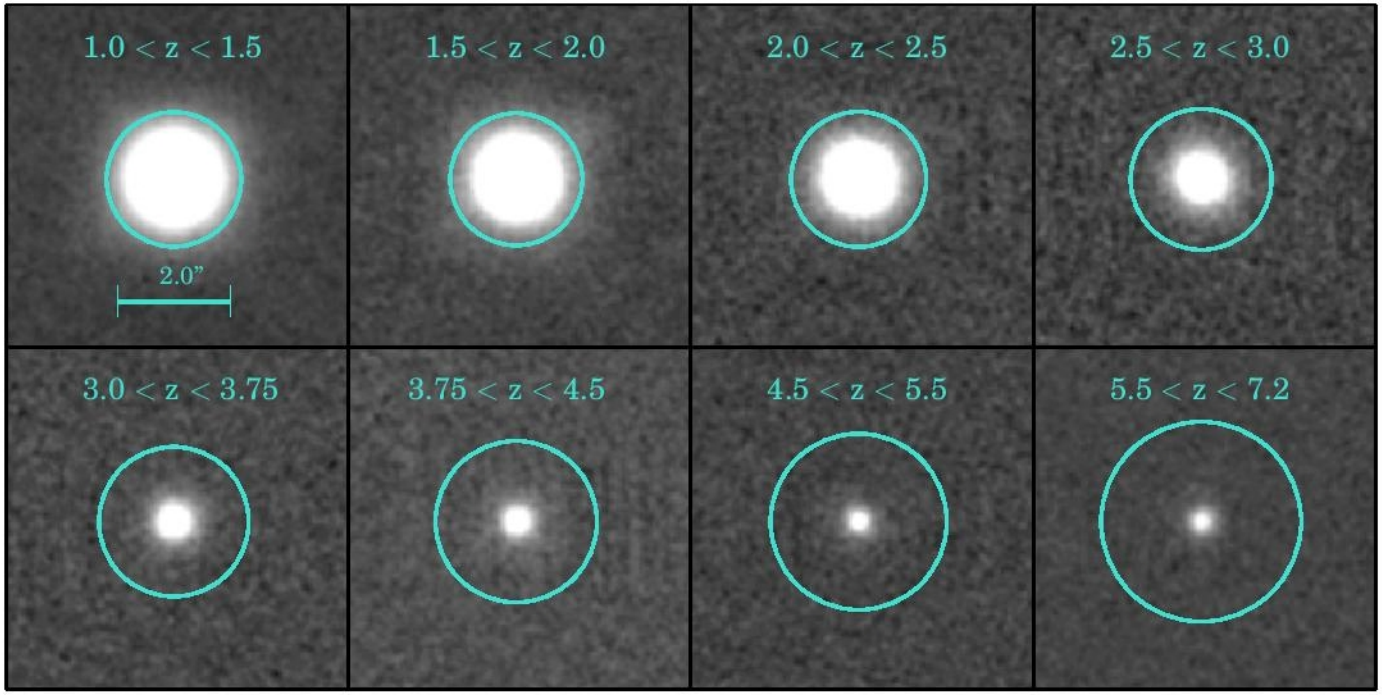

Figure 2. Stacks of galaxy images from *HST*/F160W CANDELS imaging. Each galaxy image is normalised by its F160W flux before being stacked. The circles in each panel have a diameter of 10 kpc at the stacked redshift. Note the apparent decrease in brightness and

Сравнение с эволюцией размеров Ly-break галактик

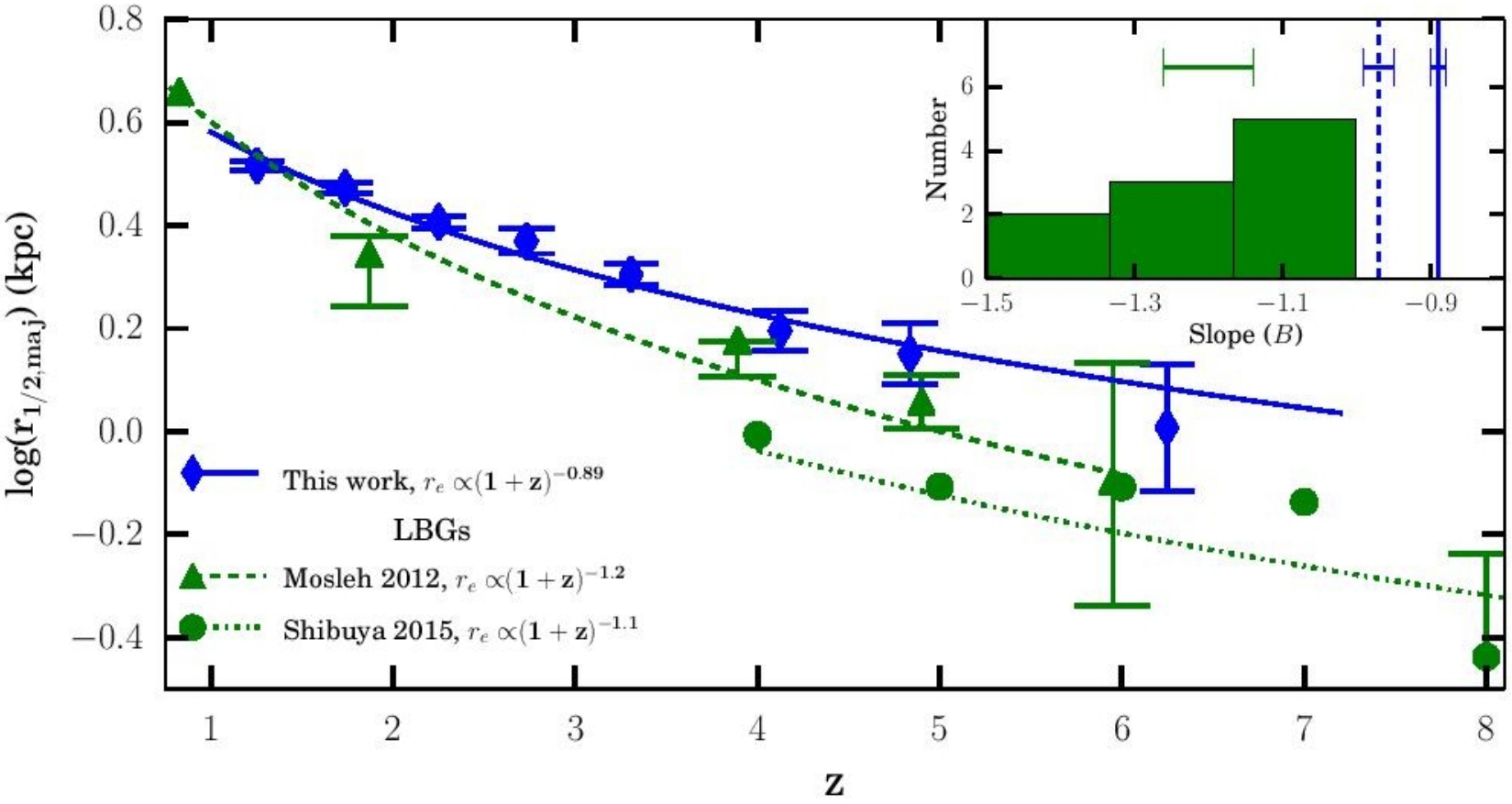

Astro-ph: 1612.05189

TESTING THE UNIVERSALITY OF THE STELLAR IMF WITH *CHANDRA* AND *HST*

D. A. COULTER,[1,2] B. D. LEHMER,[3] R. T. EUFRASIO,[2,3] A. KUNDU,[4] T. MACCARONE,[5] M. PEACOCK,[6] A. E. HORNSCHEMEIER,[2] A. BASU-ZYCH,[2] A. H. GONZALEZ,[7] C. MARASTON,[8] & S. E. ZEPF[5]

Draft version December 16, 2016

ABSTRACT

The stellar initial mass function (IMF), which is often assumed to be universal across unresolved stellar populations, has recently been suggested to be "bottom-heavy" for massive ellipticals. In these galaxies, the prevalence of gravity-sensitive absorption lines (e.g. Na I and Ca II) in their near-IR spectra implies an excess of low-mass ($m \lesssim 0.5\ M_{\odot}$) stars over that expected from a canonical IMF observed in low-mass ellipticals. A direct extrapolation of such a bottom-heavy IMF to high stellar masses ($m \gtrsim 8\ M_{\odot}$) would lead to a corresponding deficit of neutron stars and black holes, and therefore of low-mass X-ray binaries (LMXBs), per

Выборка маломассивных галактик ранних типов

Table 1
Properties of Low-Mass Elliptical Galaxy Sample

Source Name	D	σ	a	b	$\log L_K$	N_H	*HST* ACS Data		t_{exp}	N_{LMXB}	$N_{X,GC}$	$N_{X,bkg}$
	(Mpc)	(km s^{-1})	(arcmin)		(log $L_{K,\odot}$)	(10^{20} cm^{-2})	(Blue Filter)	(Red Filter)	(ks)	(field)	(GCs)	(Background)
(1)	(2)	(3)	(4)	(5)	(6)	(7)	(8)	(9)	(10)	(11)	(12)	(13)
NGC 4339	16.0	100.0	1.3	1.1	10.3†	1.62	F606W	—	33.6	2†	0†	1†
NGC 4387	17.9	97.0	0.9	0.6	10.2	2.73	F475W	F850LP	38.7	1	0	1
NGC 4458	16.4	85.0	0.9	0.7	10.0	2.63	F475W	F850LP	34.5	2	0	1
NGC 4550	15.5	110.0	1.3	0.5	10.2	2.60	F475W	F850LP	25.8	6	1	1
NGC 4551	16.1	95.0	1.1	0.7	10.2	2.59	F475W	F850LP	26.6	0	1	0
NGC 7457*	12.9	78.0	2.6	1.4	10.3	5.49	F475W	F850LP	37.7	1	0	2
Total Sample										**12**	2	6

Количество рентгеновских источников не зависит от массы галактики

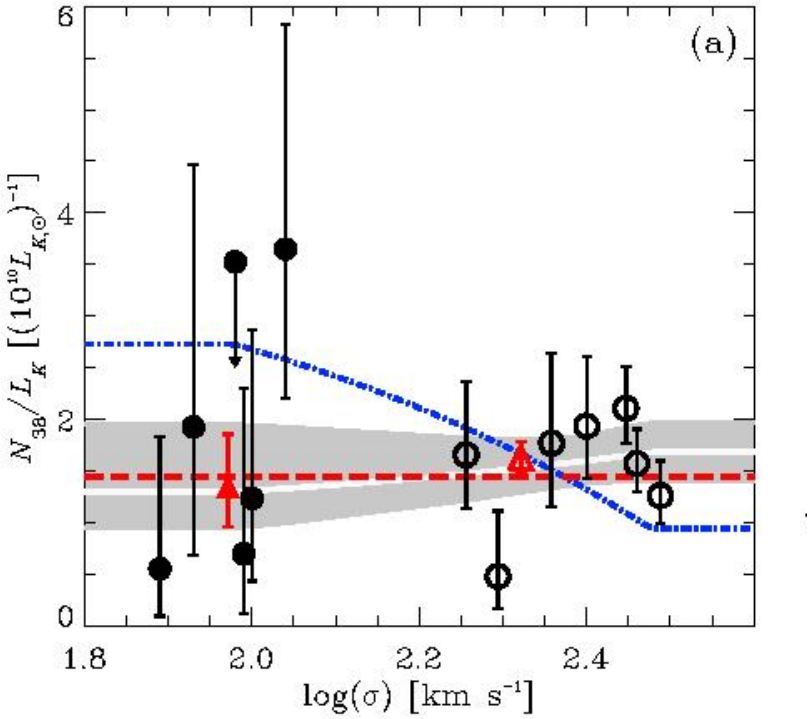

Figure 1. (*a*) The number of field LMXBs with $L_X \geq 10^{38}$ erg s^{-1} per 10^{10} L_K

Astro-ph: 1612.03171

Galactic disc profiles and a universal angular momentum distribution from statistical physics

Jakob Herpich[1⋆†], Scott Tremaine[2], Hans-Walter Rix[1]
[1] *Max-Planck-Institut fr Astronomie, Knigstuhl 17, 69117, Heidelberg, Germany*
[2] *Institute for Advanced Study, Princeton, NJ 08540, USA*

13 December 2016

ABSTRACT
We show that the stellar surface-brightness profiles in disc galaxies—observed to be approximately exponential—can be explained if radial migration efficiently scrambles the individual stars' angular momenta while conserving the circularity of the orbits and the total mass and angular momentum. In this case the disc's distribu-

Аналитический подход

The total potential energy of the disc can be written as

$$U = 2\pi \int \mathrm{d}R\, R\Sigma(R)\Phi_h(R) + 2\pi^2 \int \mathrm{d}R\, \mathrm{d}R'\, RR'\Sigma(R)\Sigma(R')W(R,R'); \quad (4)$$

here $\Sigma(R)$ is the surface density of the disc at radius R, $\Phi_h(R)$ is the gravitational potential due to the dark halo, and the kernel $W(R,R')$ is the gravitational potential between two coplanar rings of unit mass at R and R'; two expressions for this kernel are

$$W(R,R') = -\frac{2G}{\pi(R+R')} K\left(\frac{2\sqrt{RR'}}{R+R'}\right), = -\frac{2G}{\pi R_>} K\left(\frac{R_<}{R_>}\right), \quad (5)$$

where K is a complete elliptic integral and $R_<$ and $R_>$ are respectively the smaller and larger of R and R'. The gravitational potential in the disc plane is

$$\Phi(R) = \Phi_h(R) + 2\pi \int \mathrm{d}R' R' \Sigma(R') W(R,R') \quad (6)$$

and the kinetic energy of the disc is

$$T = \pi \int \mathrm{d}R\, \Sigma(R) R^2 \frac{\mathrm{d}\Phi}{\mathrm{d}R}. \quad (7)$$

The surface density is related to the distribution function by

$$\Sigma(R) = \frac{m}{R} F(j) \frac{\mathrm{d}j}{\mathrm{d}R}, \quad (8)$$

$$j^2(R) = R^3 \frac{\mathrm{d}\Phi}{\mathrm{d}R}. \quad (9)$$

2.4 The maximum-entropy disc

The maximum-entropy state consistent with a fixed number of stars N and fixed total angular momentum J is determined by the variational equation

$$0 = \delta\mathfrak{S} - \alpha\delta N - \beta\delta J = -2\pi \int \mathrm{d}j\, \delta F(j) \big[(1 + \log F(j)) + \alpha + \beta j\big], \quad (10)$$

where α and β are Lagrange multipliers. The solution to this equation is $F(j) = \exp(-1-\alpha-\beta j)$. Substituting back into equations (2) and (3) it is straightforward to determine α and β and rewrite the distribution function as

$$F(j) = \frac{N}{2\pi\langle j\rangle} \exp\big(-j/\langle j\rangle\big). \quad (11)$$

The fraction of stars with angular momentum less than j is

$$\frac{N(<j)}{N} = 1 - \exp\big(-j/\langle j\rangle\big). \quad (12)$$

Equation (11) or (12) encapsulates a remarkable result:

По экспоненте вдоль радиуса распределен момент, а поверхностная плотность – только при плоской кривой вращения

We can then compute the surface-density profile from equations (8) and (11),

$$\Sigma(R) = \frac{mN}{2\pi R\langle j\rangle} \exp\left[-\frac{Rv_c(R)}{\langle j\rangle}\right]\left[v_c(R) + R\frac{\mathrm{d}v_c}{\mathrm{d}R}\right], \quad (14)$$

An alternative form is

$$\Sigma(R) = \frac{M}{2\pi R R_e(R)} \exp\left[-\frac{R}{R_e(R)}\right]\left(1 + \frac{\mathrm{d}\log v_c}{\mathrm{d}\log R}\right), \quad (15)$$

with $R_e(R) \equiv \langle j\rangle / v_c(R)$ and $M \equiv Nm$ the total mass of the disc.

For a flat rotation curve, $v_c(R) = \text{constant}$, R_e is independent of radius and we have

$$\Sigma(R) = \frac{M}{2\pi R_e^2} \cdot \frac{R_e}{R} \exp\left(-\frac{R}{R_e}\right), \quad (16)$$

The surface density is an approximately exponential function of radius for $R \gg R_e$, and is $\propto R^{-1}$ for $R \ll R_e$. Alternatively we may ask for what rotation curve the maximum-entropy angular-momentum distribution (11) has a Freeman surface-density distribution, $\Sigma_\star(R) \propto \exp(-R/R_{\rm exp})$. It is straightforward to show that in this case

$$v_c(R) = v_\infty\left[1 - \frac{R_{\rm exp}}{R}\log(1 + R/R_{\rm exp})\right], \quad (17)$$

where $v_\infty \equiv \langle j\rangle / R_{\rm exp}$ is the circular speed at large radii.

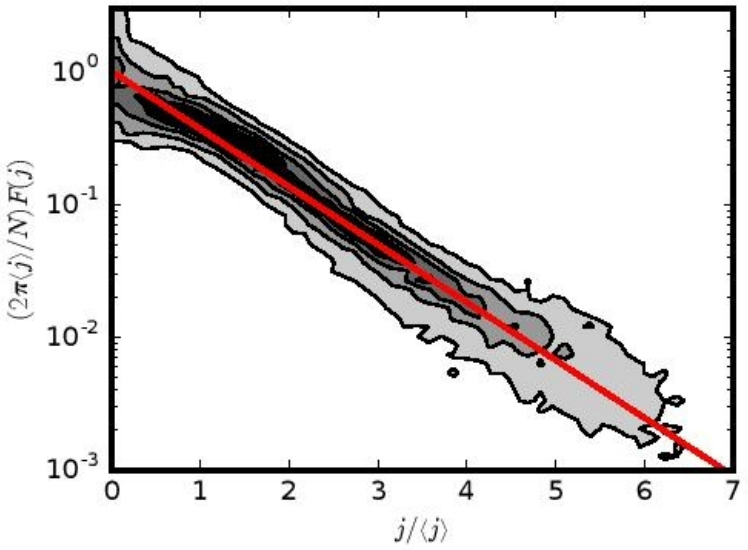

Figure 1. The distribution of specific angular momentum stacked for 304 disc galaxies from Courteau (1996, 1997). Every distribution has been rescaled using two fit parameters (normalization and $\langle j\rangle$). The contours enclose 30, 50, 70 and 90% of the plotted data points. The red line is the maximum-entropy distribution (eq. 11). Despite some small but systematic deviations for small j there is good agreement with the model prediction.